HiSST: 2nd International Conference on High-Speed Vehicle Science Technology
11–15 September 2022, Bruges, Belgium

Qualification Tests of the Actuation System of the HEXAFLY-INT Hypersonic Glider

Lucas Galembeck [1], Breno O. Silva[1], Waldemar Rotärmel[2], Sébastien Theis[3], Pasquale Manzo[4], D. Titomanlio[5], Johan Steelant[6]

Abstract

This paper deals with the qualification tests of the Actuation System of the elevons of the HEXAFLY-Int hypersonic glider. After a brief description of the design proposed by ESA and DLR, this paper successively presents the test benches and results of the different tests campaigns: (i) Mechanical test of the torsion bar at DLR-St (ii) Functional tests of the ECU and actuator at ISP-System (iii) Vacuum test of the actuator and ECU at ISP-System (iv) Vibrations and maximum hinge moment tests at ISP-System (v) Kinematical and mechanical deformation tests at Marotta (vi) GNC tests at Marotta. In addition to checking of mechanical and thermal strength, the results emphasize the levels of performance obtained in terms of maximum allowable hinge moment, rotational speed, rotational acceleration, accuracy, natural frequency with respect to the GNC requirements necessary for the completion of the HEXAFLY-Int flight experiment.

Keywords: *Actuation System, Ground tests, GNC*

Nomenclature

CMC	Ceramic Matrix Composite
DAS	Data Acquisition System
ECU	Electronic Control Unit
EFTV	Experimental Flight Test Vehicle
ESM	Experimental Service Module
FCC	Flight Control Computer
GNC	Guidance Navigation Control
LSI	Liquid Silicon Infiltration
PMS	Power Management Systema

Greek
δ_n – Elevon Deflection
t – Characteristic time constant
ξ – Damping constant

Superscripts
H – A superscript

Subscripts
w – time constant of the complex pair of poles
p – time constant of the associated pole
d – transport delay

[1] *IEAV, Aerothermodynamics and Hypersonic Division, Trevo José Alberto Albano do Amarante, n° 1 12.228-001, São José dos Campos, Brazil, galembeck@fab.mil.br; brenobos@fab.mil.br*
[2] *DLR e.V., Pfaffenwaldring 38-40, 70569 Stuttgart, Germany, waldemar.rotaermel@dlr.de*
[3] *ISP-Sytem, Z.I. La Herray, 65500 Vic-en-Bigorre, France, sebastien.theis@isp-system.fr*
[4] *Marotta S.R.L., Viale Guglielmo Marconi, 18, 80040 Cercola NA, Italia, pmanzo@marottasrl.it*
[5] *Techno System Developments S.R.L., Strada Provinciale per Pianura, 2, 80078 Pozzuoli NA, Italia, dtitomanlio@tsd-space.it*
[6] *ESA-ESTEC, Flight Vehicles and Aerothermodynamics Engineering Section , P.O. Box 299, Noordwijk, Netherlands, Johan.Steelant@esa.int*

1. Introduction

The HEXAFLY-INT vehicle is a 3 m long hypersonic glider to be launched on top of the Brazilian single stage sounding rocket VSB-50 up to an altitude of around 100 km. At the apogee, the Experimental Flight Test Vehicle (EFTV) will be released and will perform a first part of the descent trajectory aided by an Experimental Service Module (ESM). After separating the ESM, it will perform a pull-out maneuver, to finally start a gliding phase at Mach 8 at an altitude of nearly 30 km during few hundreds of seconds. The glider aeroshape design makes maximum use of databases, expertise, technologies and materials elaborated in previously European Community co-funded projects LAPCAT I & II [1][2], ATLLAS I & II [3][4] and HEXAFLY [5]. First achievements of the project are described in [6].

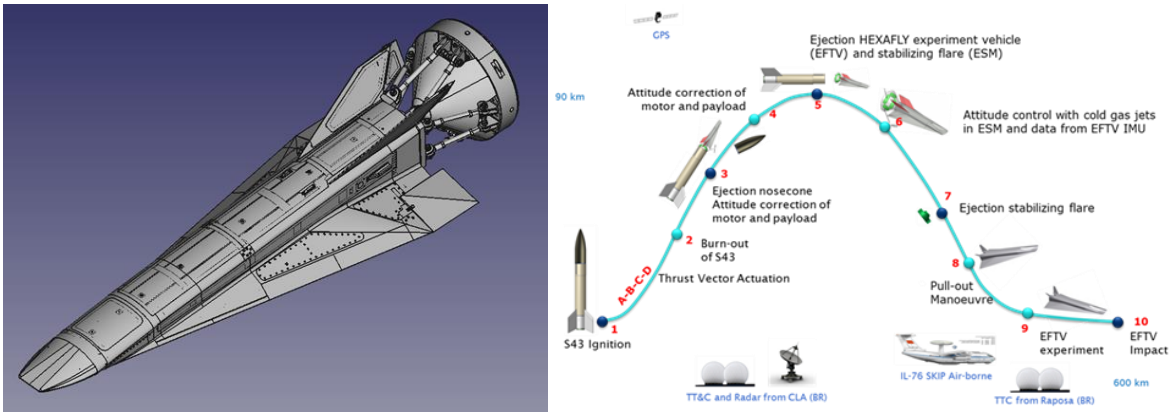

Fig. 1 HEXAFLY-INT EFTV+ESM and mission profile

The Actuation System must ensure the correct positioning of the elevons within specified tracking performances and be able to guarantee these performances despite disturbances and uncertainties that may affect the positioning accuracy (i.e., mechanical yokes, transducer accuracy and so on). The Actuation System was then required to fulfil the following tracking requirements on the basis of preliminary GNC recommendations [7]:

- Steady state error (bias) and static accuracy ≤ ±1°;
- Natural frequency ≥ 100 rad/s (16 Hz) (equivalent 1st order time constant ≤ 0.01 s);
- Damping factor ≈ 0.7;
- Latency ≤ 0.02 s;
- Dead zone and backlash ≤ ± 0.1°.

In addition, the following dynamic requirements were defined by CIRA:

- Maximal angular speed ≥ 20°/s
- Maximal angular acceleration ≥ 700°/s^2

The maximum required hinge moment should be at least higher than 332 Nm. It is mainly defined by the mechanical strength of the torsion bar of the Actuation System and then used as a constraint by the GNC laws.

2. Actuation System design

The Actuation System was elaborated and designed as already presented in [7]. It is mainly based on a deported pressurized Electronic Control Unit (ECU), a linear servo-actuator, a titanium lever arm, a mixed titanium/CMC torsion bar, a CMC elevon, and a thermal protection jacket based on Aeroguard® material (Fig. 2). All other parts forming the attachments of the Actuation System with the internal airframe, the fuselage, the wings are made in titanium. The ECU and actuator were designed and manufactured by ISP-System, the CMC parts were designed and manufactured by DLR-St, the titanium parts were designed by the different partners and manufactured by Marotta. Finally, the thermal protection jacket was designed and manufactured by PROMAT on the basis of ESA sizing.

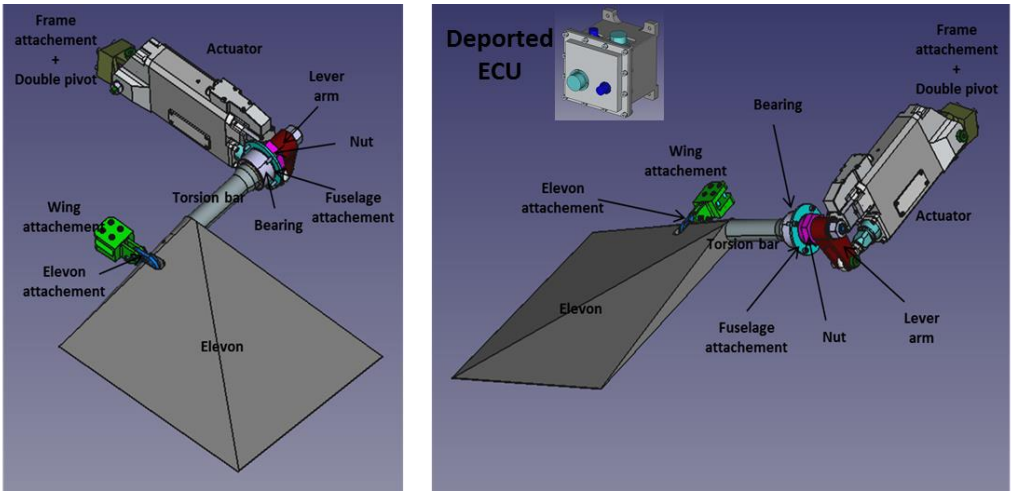

Fig. 2 Actuation System design (without thermal protection)

3. Mechanical tests of the CMC torsion bar

Some stand-alone tests of the torsion bar were performed by DLR-St on their torsion test rig (Fig. 3), so as to determine its torsional deformation, the repeatability of the mechanical deformation with respect to fatigue, and finally the maximum allowable hinge moment which is a critical input for GNC. The CMC material is a C/C-Sic material using the LSI process during manufacturing.

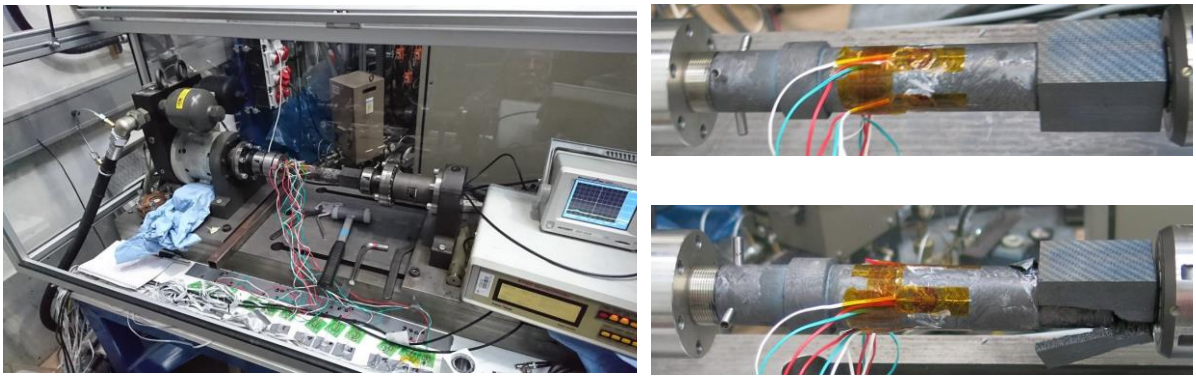

Fig. 3 Torsion test rig with CMC torsion bar mounted with representative interfaces included

The torsional stiffness of the torsion bar assembly was found to be nearly 10 000 Nm without any influence of fatigue. The maximum allowable hinge moment was determined as nearly 330 Nm. The breaking of the assembly appears at the interface with the elevon.

4. Modular ground test bench of the full activation lane

A modular ground test bench was designed and manufactured by ISP-System so as to check the functionalities of the actuator and ECU in terms of amplitude, speed and acceleration of the motion while some hinge moment (up to the critical value) is applied at the extremity of the torsion bar. The test bench was designed to be modular allowing inclusion of the elevon and its wing-mounting as well as an overall representative system for environmental testing, i.e., thermal, vibrational… for qualification and acceptance tests.

The aerodynamic moment on the torsion bar and the activation lane is represented and applied thanks to a torque resulting from the deformation of a copper bar aligned with the torsion bar and fixed on

the bench at its extremity (Fig. 4). At first, a steel torsion bar instead of the titanium/CMC bar was used to test out the ECU and actuator. It did not include the elevon and its attachment to the wing.

In addition to the information provided by the ECU (actuator's rod position, speed, acceleration, …), a load sensor was placed on the frame attachment to measure the longitudinal load applied on the actuator and an angular position sensor was placed at the interface between the lever arm and the torsion bar to measure the angular motion of the lever arm. Some measurement of voltage and current provided by the ECU complete the test bench sensors.

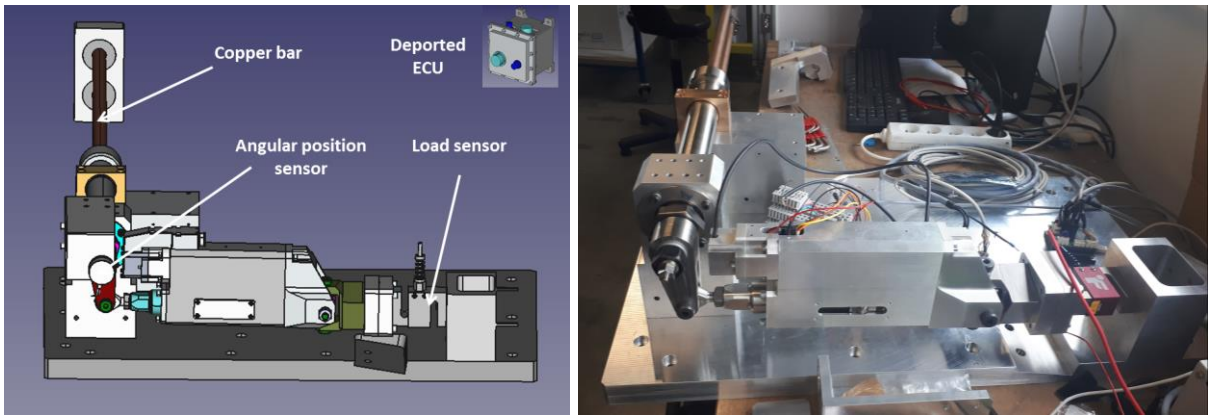

Fig. 4 Modular test bench for functional tests of the actuator and ECU

The actuator and its ECU were found to fulfil their requirements if enough current was provided (up to 30 A is necessary when maximal load, speed and acceleration are combined). The allowable embedded current becoming the most critical limitation of the Actuation System, some parametric tests were performed so as to develop a semi-empirical model of power consumption with respect to load, speed and acceleration. This model will be used for the improvement of the Power Management System (PMS) by TSD.

5. Vacuum tests

The same modular test bench was used in vacuum conditions to check the mechanical strength of the pressurized ECU and the thermal strength of all components with respect to their own heating by Joule effect. The tests include also the first 20 minutes of the pre-launch operations when the ECU and actuator are just switched ON, followed by a series of commanded motions which are very conservative in terms of consumed power with respect to the reference flight trajectory.

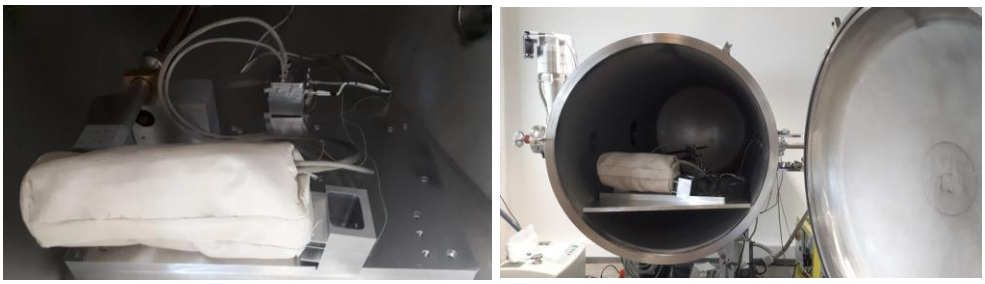

Fig. 5 Preliminary test bench (including its thermal protection jacket) inside the vacuum chamber

No air leak was found for the ECU box. The thermocouples placed on the ECU electronic cards, ECU box, actuator motor and thermal protection jacket did not result into temperatures higher than 40°C at the end of the test (the initial temperature was nearly 24°C).

6. Environmental tests

The complete test bench includes all parts of the Actuation System: the mixed titanium/CMC torsion instead of the preliminary steel bar, a dummy CMC elevon (i.e., a representative CMC elevon with all essential interfaces included but limited in streamwise length) and the attachment with the wing. The mechanical strength of the system with respect to the vibrations during the boosted phase of the flight and with respect to the maximum hinge moment during the glided phase of the flight is checked followed by a final characterization of the complete system at Marotta premises. The test bench is placed on a vibration table by means of an inclined stiff metallic platform to assure the right attitude position w.r.t. the launcher loads. The strength with respect to sinusoidal and random vibrations is performed along the three directions. For the qualification tests with the CMC dummy elevon, a steel extension plate is attached to it to correctly represent the inertia of the full elevon (see Fig. 6). Acceptance tests are performed with the fully sized flight elevon.

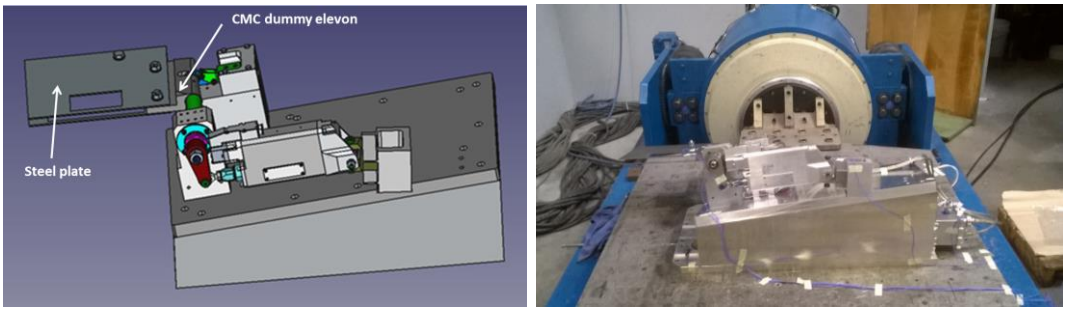

Fig. 6 Vibrations tests of the full Actuation System

For the post-functional test, the additional steel plate is then removed (Fig. 7), and the hinge moment is applied on the dummy CMC elevon in a way similar to the pre-functional tests. Tests assessing the strength with respect to the maximum hinge moment defined by DLR-St (330 Nm) are ongoing.

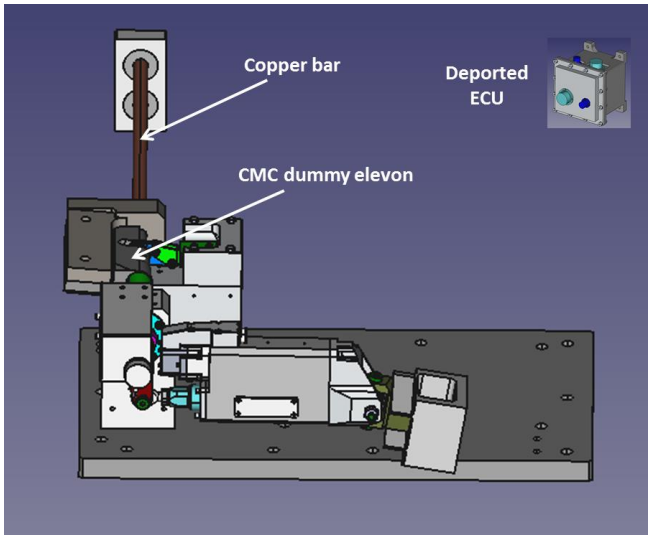

Fig. 7 Final test bench of the full Actuation System

7. Kinematics, mechanical deformation, GNC tracking tests

The modular test bench is assessed at Marotta premises to characterize more deeply and precisely the kinematical law, the GNC tracking performances, the mechanical deformations, and mechanical backlashes. A dedicated Real Time Actuation and Acquisition System was developed by TSD to emulate the Flight Control Computer (FCC) to command the actuator with any type of signals, and, in addition, to work as a DAS (Data Acquisition System) to synchronize all the different sensors' data (Fig. 8).

An additional angular position sensor placed on the elevon also completes the measurements of the modular test bench. The test campaign will include quasi-steady motions but also dynamic motions. While the CMC torsion bar is being produced for the qualification tests, a characterization campaign of the actuation system is done with the metallic torsion bar. Changing the fixation position of the copper bar (Fig. 7) enables altering its stiffness level and adjusting the Hinge Moment (HM) loading conditions of the tests.

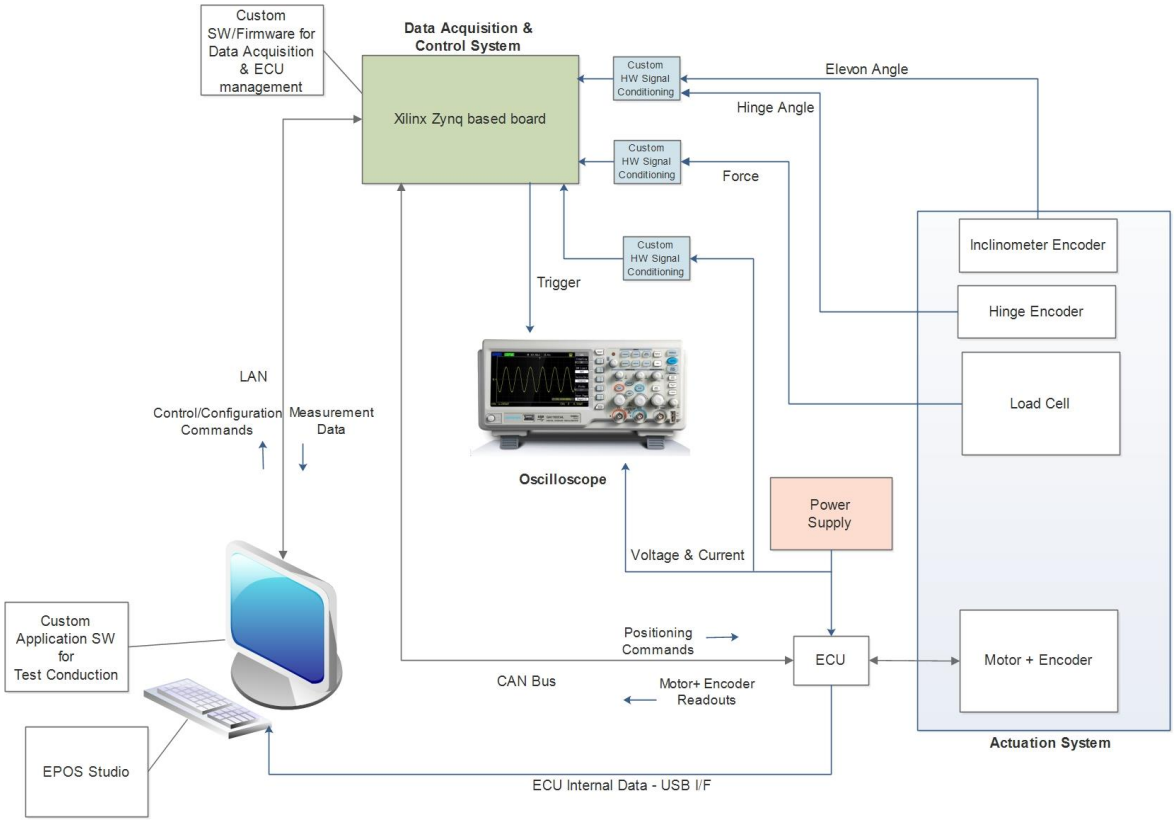

Fig. 8 DAS real-time architecture for the actuation system

The test campaign objective is to evaluate the Actuation System characteristics, in a static (or quasi-static) and in a dynamic way:

I. Static Tests:
   a. Input-Output (IO) map
   b. Static accuracy
   c. Random accuracy (zero-mean Gaussian noise)

II. Dynamic Tests:
   a. Dynamic Transfer Function (TF): time constant (1st order) or natural frequency and damping coefficient (2nd order), depending on the tradeoff between accuracy and complexity.
   b. Dead band
   c. Delay or latency time
   d. Backlash
   e. Phase delay
   f. Saturations: Max/min angular deflections (saturations), Max/min angular rates (slew rates), Max/min angular accelerations

It is worth noting that the evaluation of the "tracking performance" of the Actuation System is intended end-to-end, i.e. from the angular command up to the elevon angular deflection. This is not equivalent to analyze the linear displacement of the rod because:

- the deformation effects (downstream from the linear sensor) must be taken into account;

- the angular/linear map could be nonlinear, therefore the dynamic system characteristics could significantly change analyzing only the servo-actuator subsystem.

For the first feature, i.e., IO map, a series of internal conversions is mapped so the user can directly work with the inputs and outputs in degrees. The ECU works only in terms of the actuator's motor internal quadrature counts (qc). They can be converted straightforwardly in the rod's linear displacement (1 qc = 156.25μm). The rod's displacement, on the other hand, needs to be converted into an equivalent elevon deflection using a highly non-linear equation (1) derived from **Erro! Fonte de referência não encontrada.**

$$\theta_{elevon} = \gamma_0 - \operatorname{acos}\left(\frac{a^2 + b^2 - (c_0 - x_{rod})^2}{2\,ab}\right) \quad \textbf{(1)}$$

It is important to notice that this relation is highly dependent of the parts' measurements and small dimensional errors will give inaccurate results. To reduce numerical errors, all the test bench components real dimensions are measured with a high precision machine.

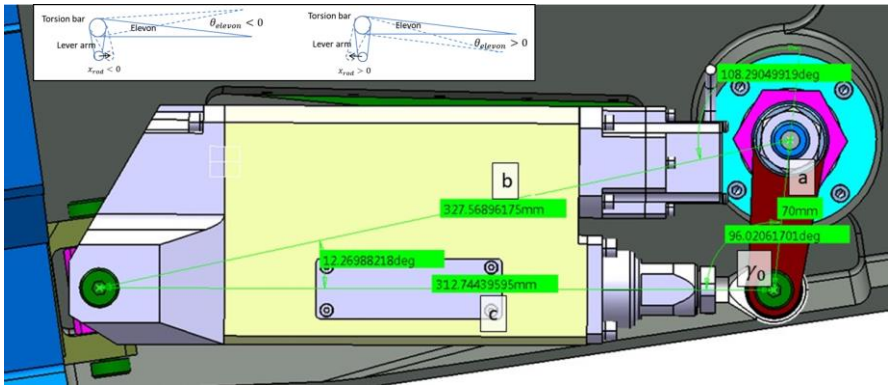

Fig. 9 Lateral view of the actuator and convention for the linear to angular conversion

The conversion from the rod's linear displacement (mm), or its internal counts (qc), to the expected deflection (degrees) can be seen on Fig. 10. In addition, on the right axis (orange) it is possible to notice how this relation is nonlinear. In any case, the expected deflections (in °) can be easily computed, programed in the FCC, and will be used straightforwardly to command the actuator from this point onwards.

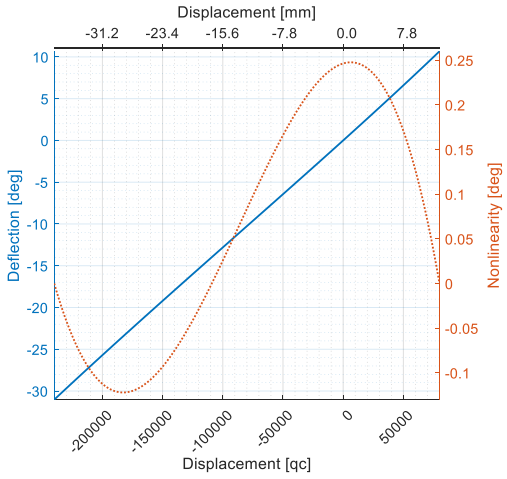

Fig. 10 IO map (qc or mm to degrees)

With a series of step inputs going from -30° to +10° with 2° steps, it was possible to assess the static accuracy of the system. The data was collected 5 seconds after the final position was reached. It is important to say that the output error at the actuator level is neglectable (≤0.01°) for all the gains and loading conditions and the analysis was focused at the elevon output. Fig. 11 shows the output errors

for several loading conditions. The right figure focus on the error caused by the deformation of the actuation system when exposed to load.

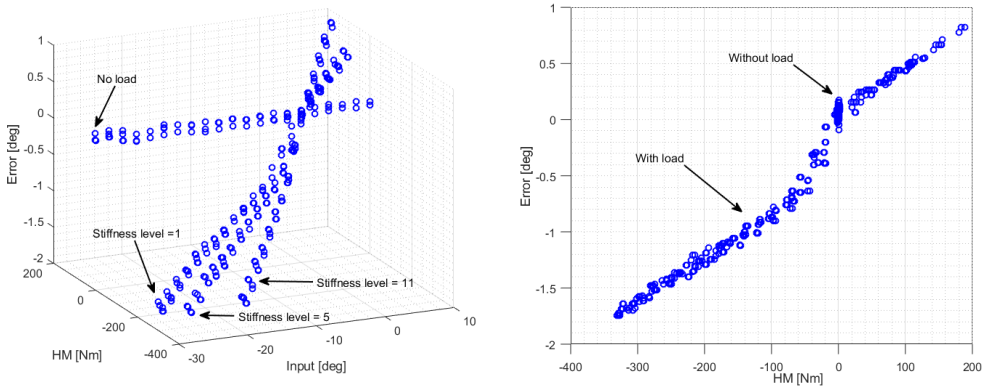

Fig. 11 Output errors (°) after steady state conditions are reached as a function of the inputs and HM (left) and only as a function of the HM (right)

With these results, a deformation model was estimated and used to de-trend the output errors. After that, the residual error (subtracting the elevon's output error from the expected deformation) can be analyzed easily (Fig. 12). The same process was repeated later using random inputs to estimate the random accuracy. The static accuracy for the cases with load can be estimated as 0.00±0.05° and the random accuracy as 0.01±0.06°. The largest dispersions are in the region close to zero, where the main errors are probably not due to deformation, but due to backlashes and other nonlinearities that will be dealt below. The small offset in the random case could have been caused because a relative sensor is being used, so the initial alignment does not match exactly the zero (neutral) position. In any case, the residual errors are always smaller than 0.2° showing that this deformation model is good to balance the effect of the deformation due to the hinge moments.

Table 1 - Linear regression model of the deformation as a function of the HM.

f(x)=a*x+b	HM ≤ -40Nm	-40Nm < HM ≤ 0	0 < HM
Coefficient a	0.0039	0.0140	0.0041
Coefficient b	-0.4550	0.0495	0.0495
R^2	0.9840	-	0.9704

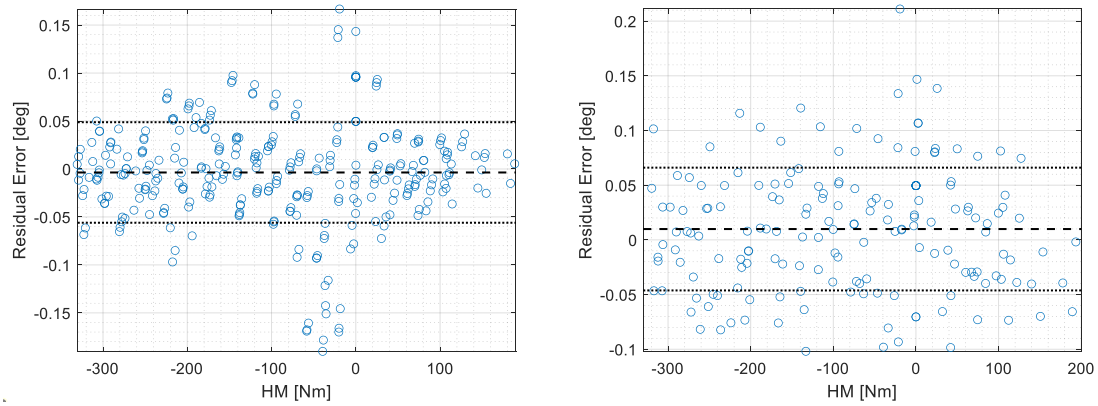

Fig. 12 Static (left) accuracy (0.00±0.05°) and random (right) accuracy (0.01±0.06°) for the cases with load after removing the estimated deformation

For the Dynamic TF, a series of ±0.4° step inputs were commanded with different loading and gain conditions. This value was chosen to be a compromise between a small amplitude movement (to remain as close as possible to the linear dynamics) and the sensors sensitivity considering its accuracy and the nonlinear mechanics acting on the actuation lane (backlash, hysteresis, etc.). Smaller amplitudes would

not allow the real characterization of the complete movement because the nonlinearities would have the same order of magnitude of the full step amplitude. Larger amplitudes would enhance the nonlinearities of the system response making the linear theory completely not applicable. The TF coefficients were obtained passing the responses in a numerical optimization to fit the first and second-order models (P1D, P2D and P2DU) as defined in the *procest* function in Matlab [8] and in equation 2. Fig. 13 shows an example of the system response with maximum stiffness level and different gains (left) and the fittest model (2nd order underdamped system) in the right figure. On Table 2 it is possible to see the average coefficients considering the fittest model for each gain set programmed in the controller. With these values it is already possible to create a mathematical model in Matlab that is able to reproduce most of the system's behavior. Although, to have a more realistic model it is necessary to model also the nonlinear characteristics of the system. An estimation was done for the system backlash, latency, dead zone and saturation.

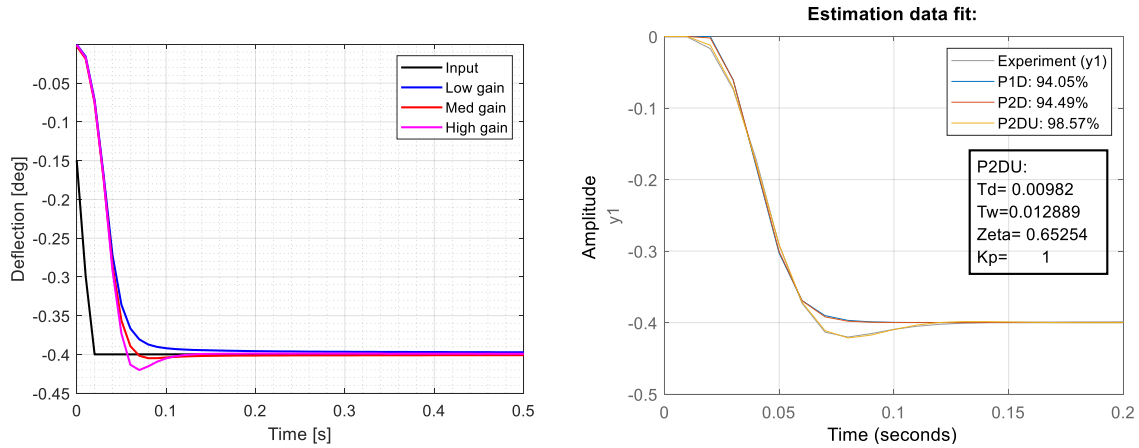

Fig. 13 Left: System's response for different gains with a stiffness level of 11. Right: Model comparison for a -0.4º step input (zoom: 0.2 sec) with stiffness level 11 and high gain

Table 2 – Summary with the TF model's coefficients estimated values

Gain	Type	Parameter	Mean	Accuracy	Unit
High	P2DU	t_w	0.013	±0.001	s
		ξ	0.832	±0.081	
		t_d	0.011	±0.001	s
Medium	P2D	t_{p1}	0.023	±0.004	s
		t_{p2}	0.004	±0.001	s
		t_d	0.011	±0.004	s
Low	P1D	t_{p1}	0.027	±0.007	s
		t_d	0.012	±0.001	s

$$P1D: sys = \frac{e^{-\tau_d s}}{1+\tau_{p1} s}$$

$$P2D: sys = \frac{e^{-\tau_d s}}{(1+\tau_{p1} s)(1+\tau_{p2} s)} \quad \textbf{(2)}$$

$$P2DU: sys = \frac{e^{-\tau_d s}}{1+2\xi\tau_w s+(\tau_w s)^2}$$

The backlash was estimated using a sinusoidal input (10º at 0.1Hz) associated with load on the actuator. Fig. 14 shows an example of the method used to estimate the backlash with load. Focusing on the HM curve, it is possible to notice that in the regions with change of direction, there is a nonlinear leap on the moment curve. This happens because when there is a change in direction, the mechanical parts travels freely for a few millimeters until the air gap between the links and connections is closed. During

this phase, the load cell senses an instantaneous relief that can be seen on the HM curve as a drop or increase on the measured levels. In this method, we use this temporary relief to estimate when we have the backlash acting. Identifying the instant that the backlash started and stopped to act in comparison to the deflection, it is possible to have a measurement of this free mechanical gap in degrees (backlash). After a series of experiments, an average backlash of 0.06 ± 0.02º was obtained (with load).

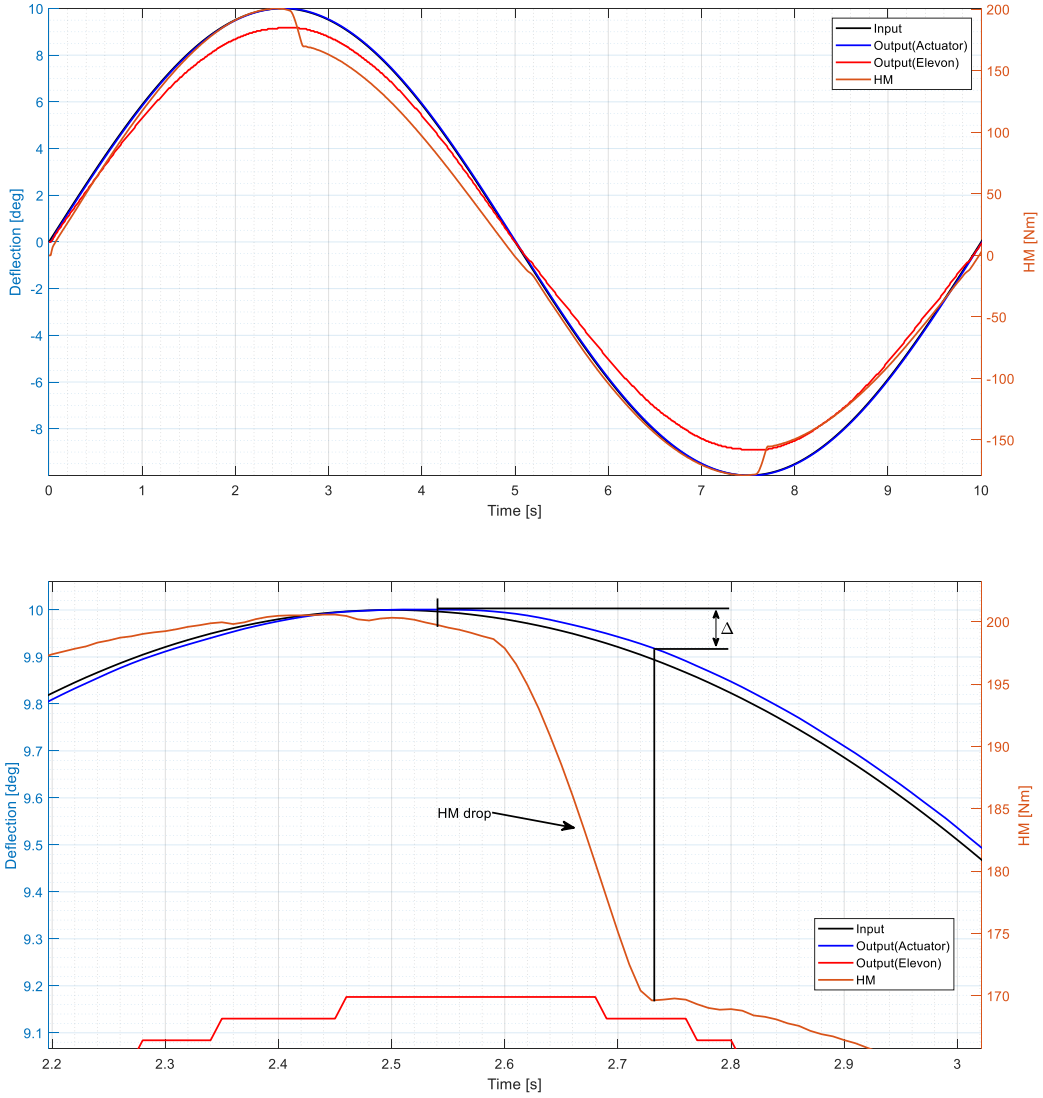

Fig. 14 Comparison of the deflection and the HM for a sine (10º – 0.1Hz) with a stiffness level 11 and a high gain condition (top) and a zoom in the upper region (bottom).

To estimate the latency and the dead zone (of the actuator) it was necessary to use the EPOS Studio (sampling time up to 1.2ms) and the ECU auxiliary USB connection in parallel to the DAQ connection since the fixed sampling frequency of the external DAQ is limited to 100Hz and 10ms seemed to be higher than the latency. It needs to be clarified that the EPOS' internal control loop response depends on the gains and on the initial conditions (e.g.: target, demand position, actual position, rpm, etc.…). In any case, it is important to understand that the internal PID positioning controller works on a 2.5KHz frequency (400µs). It is possible to see that the internal control variables are changing accordingly to the control loop frequency, but it takes some milliseconds until we get a quantifiable output. With respect to the actuator output, the response depends on several factors, but considering an average behavior it starts when the difference between the internal loop variables, demand and actual position (in increments), gets higher than 8±2 inc (equivalent to 0.001 ± 0.0002º) which gives us a latency or delay smaller than 11±2ms for a really small ramp input with a 0.1º /s slope. It is important to

understand that it does not mean that before this interval nothing happens, this is only the time it takes to get a quantifiable output on the actuator for a really small input. In any case, these levels of latency are considering a very conservative approach and the response will be faster, if we use a higher slope, but it will not be possible to identify when the movement starts. It is possible to observe that this latency level is also in agreement with the results from the second order underdamped model found above.

To estimate the saturation, a series of tests with ramps (19°/s and 20°/s) was performed moving from 0° to -30° (or the maximum allowed deflection not to exceed the HM limits with load). Table **3** shows the results for a series of tests. It is possible to see that the angular velocity saturates around 21.8°/s and the acceleration around -406°/s^2. However, it is important to remark that the tests with load started at the neutral position, so the maximum accelerations happened with very small HM levels. Other combinations of HM, acceleration and loads can create different saturation scenarios when the amperage limit is achieved. To deal with different scenario combinations and to obtain a better estimation of the angular acceleration saturation levels, an operational envelope was numerically estimated and then experimentally tested. With this model, it was possible to have a more realistic estimation of the available acceleration under different combination of load and current at the motor level. Fig. 15 Fig. 15 shows the operational envelope considering the numerical model of the motor's power consumption and maximum accelerations obtained experimentally. The maximum condition is allowed only briefly during intermittent phases of acceleration or deceleration. In a scenario without load (or with low levels of load), the acceleration can reach levels of more than 400°/s^2, but when the motor is already loaded and consuming levels of current close to the maximum (14.9A), then the acceleration will be limited to around 190°/s^2.

Table 3 - Maximum velocities and accelerations (negative direction) for a negative ramp – acceleration phase

Stiffness level	Gain	Maximum (negative direction)			
		Angular velocity (°/s)	Angular acceleration (°/s²)	Motor velocity RPM	Motor acceleration RPM/s
0	Low	-21.8196	-407.59	-9889	-133500
	Med	-21.7938	-406.29	-9885	-133500
	High	-21.8196	-407.59	-9894	-133300
1	Low	-21.9359	-412.78	-9765	-135100
	Med	-21.9230	-408.88	-9828	-134900
	High	-21.9231	-408.90	-9844	-134700
5	Low	-21.8494	-407.17	-9734	-134600
	Med	-21.8838	-410.20	-9802	-134400
	High	-21.9103	-407.59	-9825	-134900
11	Low	-21.9266	-409.79	-9732	-134500
	Med	-21.9617	-408.88	-9791	-135100
	High	-21.9617	-408.46	-9802	-135000

Additional tests were also performed to assess the GNC tracking performance. it was simulated the nominal trajectory (full duration) with medium gain and stiffness level 11. On the right axis (blue) of Fig. 16, it is possible to see the HM levels obtained at the experiment and the HM levels expected for the flight obtained from CIRA's GNC numerical simulation. It is easy to see that even with the maximum stiffness level possible with the copper bar, the HM does not match the expected profile of the HM for the flight. The first problem is that the test bench's HM is always proportional to the deflection, which is not always true in the flight as other phenomena might occur in a concurrently manner, e.g., vehicle's attitude, density and velocity variations resulting in changing dynamic pressures. Also, the test bench's HM is always a restoring moment, and in the flight the HM can act in the opposite direction (for example between 50s and 250s). This affects the overall deformation at the actuation lane giving actual elevon outputs that are larger than the commanded deflection, which is not seem in the test bench (actual deflection is always smaller than the commanded). In addition, this will also affect the motor's

performance, because during the flight, in certain conditions, the motor will not have the help of the restoring moment to achieve a new deflection. At least for the nominal trajectory, with the known HM's profile limitations in the test bench, it was observed that the motor was not close to any operational limit, and it could perform the deflections without major problems.

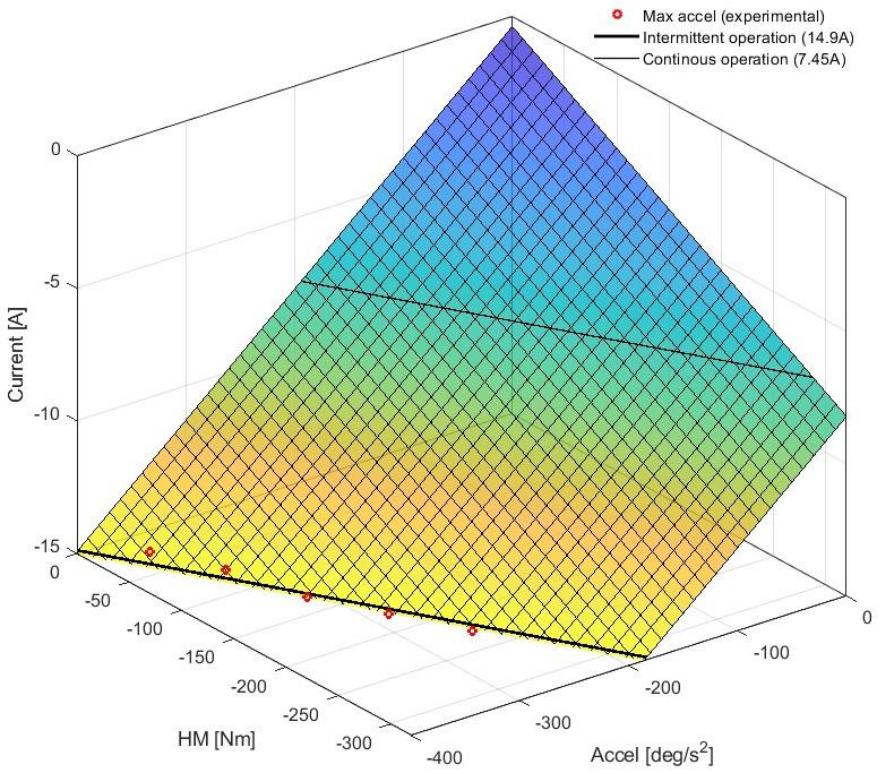

Fig. 15 Operation envelope considering the power consumption model for the actuator's internal electric motor

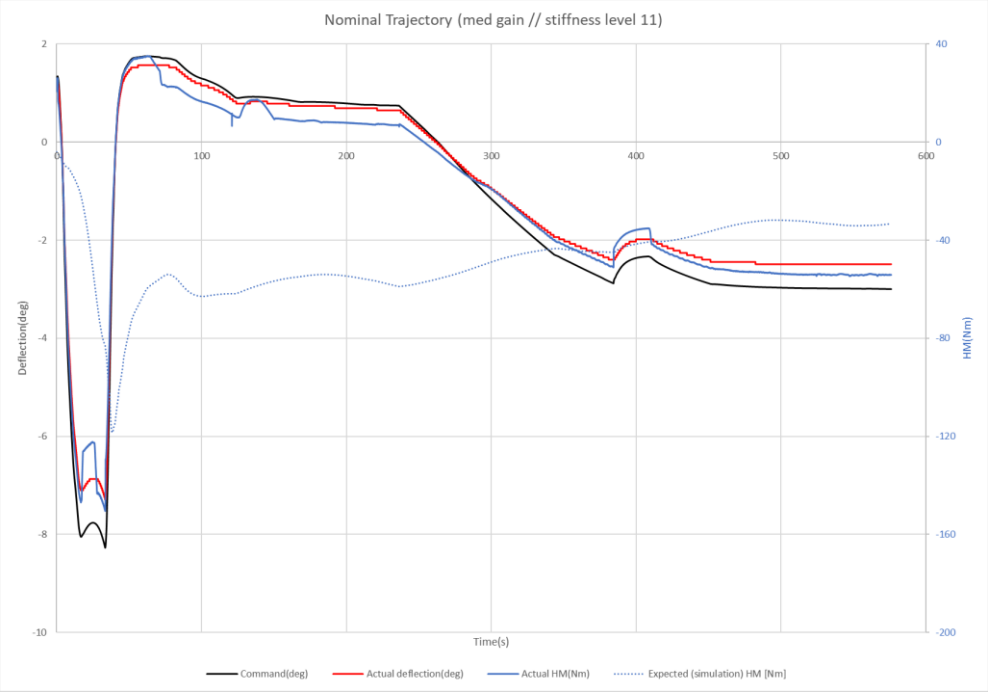

Fig. 16 Nominal trajectory simulation with medium gain and stiffness level 11.

An extra experiment was done to reproduce the nominal's trajectory HM profile. The objective here is not to emulate the flight conditions, but only to assess the mechanical strength of the actuator to deal with this specific HM profile curve. As already discussed, the limitations on the test bench does not allow a perfect reproduction of the HM curve. To deal with this, the experiment was done by parts and the deflections were computed a reverse engineering method to obtain the necessary HM. In addition, the backlash introduces a leap every time the deflection changes direction, making it very hard to compute the exact required deflection. The complete trajectory was divided into 9 parts (as seen on Fig.17) and the required deflection was computed for each step to give the closest match in the HM as possible. Small intervals of time where a sequence of direction reversions happened were ignored. The deflections and the other parameters do not have any relation with the trajectory and their assessment doesn't give any reliable information about the system's performance, this test is purely to check the ability of the actuator to endure under a more realistic HM profile.

Fig. 17: Reproduction of the nominal trajectory HM profile by parts (top) and required deflections to reproduce the nominal's trajectory HM profile by parts (bottom).

Considering the experimental characterization of the actuation system, it was possible to create a Simulink simulation model that will be used to refine the vehicle's trajectory analysis. It is important to

remember that these experiments were done with the metallic torsion bar and will have to be repeated when the CMC torsion bar is available. In any case, most of the parameters does not depend on the torsion bar and a preliminary conformity or nonconformity of each characteristic analyzed according to the requirements set for the actuation system can be seen on Table 4. Some setbacks with the actuation system delayed the completion of the tests and required that extra solutions were developed. Finally, the characterization of the actuation lane with the metallic torsion bar could be completed. The tests with the CMC torsion bar are still on hold until the problem that caused the failure is identified, solved and a new torsion manufactured. Nevertheless, the system seems to perform well for most of the conditions.

Table 4 – C/NC summary of the requirements

	Requirement	**Test**	**Compliance**
Static accuracy	≤ ±1°	0.00±0.05° (subtracting the deformation)	OK
Steady state error	≤ ±1°	≤ ±1.72° (depends on the HM)	NOK
Natural frequency	≥ 100 rad/s (16 Hz)	Step method: 12.2Hz Freq. resp. method: 5.88Hz	NOK
Damping factor	≈ 0.7	0.832±0.081	NOK
Latency	≤ 0.02 s	Epos Studio: 11±2 ms Step method: 11 ms	OK
Dead zone	≤ ± 0.1°	0.001±0.0002 deg	OK
Backlash	≤ ± 0.1°	Without load: 0.13±0.01° With load: 0.06±0.02 °	NOK OK
Range of deflection	40°	Full stroke: 41.67 ° With safe margin: 40°	OK
Maximal angular speed	≥ 20°/s	≥ 21.79 °/s	OK
Maximal angular acceleration	≥ 700°/s^2	Without load: ≥ 406.29°/s^2 With load: ≥ 190°/s^2	NOK

8. Conclusions

The main non-compliances observed during the test is related to the maximum acceleration requirement which needs to be relaxed. It could be observed that this reduced performance is related to the maximum peak amperage allowed in the actuator's electrical motor (14.9A). New GNC simulations have to be performed to assess the vehicle's response with the parameters identified. In any case, it is important to have in mind that excessive amperage for a longer duration in the electric motor can overheat the windings and damage the system.

As the actuation system is critical for the flight, it is not recommended that the current limit is exceeded. A secondary limit could also be achieved with a very critical combination of HM, acceleration and velocity that could demand more than 30A at the ECU level and although this limit was implemented in the system, it was never observed during the tests.

Future tests will soon include the vibrational tests for the qualification and acceptance of respectively the dummy and flight elevon. After these tests, the final functional characterization will provide a more representative model of the actuation system once being activated after the ascent with the sounding rocket.

References

1. Steelant J., 'Achievements Obtained for Sustained Hypersonic Flight within the LAPCAT Project', 15th AIAA International Space Planes and Hypersonic Systems and Technologies Conference, AIAA-2008-2578, 28 April- 01 May 2008, Dayton, Ohio, USA.
2. Steelant J., Varvill R., Defoort S., Hannemann K. and Marini M., 'Achievements Obtained for Sustained Hypersonic Flight within the LAPCAT-II Project', 20th AIAA International Space Planes and Hypersonic Systems and Technologies Conference, AIAA-2015-3677, 5-8 July 2015, Glasgow, Scotland.

3. Steelant J., 'ATLLAS: Aero-Thermal Loaded Material Investigations for High-Speed Vehicles', 15th AIAA International Space Planes and Hypersonic Systems and Technologies Conference, AIAA-2008-2582, 28 April-01 May 2008, Dayton, Ohio, USA.

4. Steelant J., Dalenbring M. ., Kuhn M., Bouchez M. and von Wolfersdorf J., 'Achievements obtained within the ATLLAS-II Project on Aero-Thermal Loaded Material Investigations for High-Speed Vehicles', 21st Int. Space Planes and Hypersonic Systems and Technology Conference, AIAA-2017-2393, 6-9 March 2017, Xiamen, China.

5. Steelant J., Langener T., Hannemann K., Riehmer J., Kuhn M., Dittert C., Jung W., Marini M., Pezzella G., Cicala M. and Serre L., 'Conceptual Design of the High-Speed Propelled Experimental Flight Test Vehicle HEXAFLY', 20th AIAA International Space Planes and Hypersonic Systems and Technologies Conference, AIAA-2015-3539, 5-8 July 2015, Glasgow, Scotland

6. Steelant J. et al, Flight Testing Designs in HEXAFLY-INT for High Speed Transportation, 1st International Conference on High Speed Vehicle Science Technology, 26-29 November 2018, Moscow, Russia

7. Andro J.Y, Rotärmel W. and Steelant J., Design of the Actuation System of the Hexafly-Int Hypersonic Glider, 1st International Conference on High Speed Vehicle Science Technology, 26-29 November 2018, Moscow, Russia

8. MathWorks, Documentation for the Procest function. https://www.mathworks.com/help/ident/ref/procest.html (2012). Accessed 18 October 2021